Carbohydrate Polymers 110 (2014) 18–25

Contents lists available at ScienceDirect

Carbohydrate Polymers

journal homepage: www.elsevier.com/locate/carbpol

Synthesis and characterization of graphene oxide/carboxymethylcellulose/alginate composite blend films

Mithilesh Yadav [a], Kyong Yop Rhee [a,*], S.J. Park [b]

[a] Department of Mechanical Engineering, College of Engineering, Kyung Hee University, 446-701, Republic of Korea
[b] Department of Chemistry, Inha University, 253, Nam-gu, Incheon 402-751, Republic of Korea

ARTICLE INFO

Article history:
Received 13 January 2014
Received in revised form 19 February 2014
Accepted 5 March 2014
Available online 4 April 2014

Keywords:
Sodium carboxymethylated cellulose
Graphene oxide
Tensile strength
Thermogravimetric analysis
Fourier transform infrared spectroscopy

ABSTRACT

In this work, graphene oxide/carboxymethylcellulose/alginate (GO/CMC/Alg) composite blends were prepared by a simple solution mixing-evaporation method. The resulting structure, thermal stability, and mechanical properties of the blends were investigated by wide-angle X-ray diffractometry, Fourier transform infrared spectroscopy, Raman spectroscopy, scanning electron microscopy, thermogravimetric analysis, and mechanical testing. The obtained findings revealed that CMC, Alg, and graphene oxide were able to form a homogeneous mixture. When compared to a CMC/Alg blend, the incorporation of 1 wt% graphene oxide improved the tensile strength and Young's modulus by 40% and 1128%, respectively. In addition, the GO/CMC/Alg composite blend film showed a higher storage modulus than the CMC/Alg blend.

1. Introduction

Polymeric blends are physical mixtures of structurally different polymers or copolymers that interact via secondary forces with no covalent bonding. Such interactions include hydrogen bonding, dipole–dipole forces, and the formation of charge transfer complexes for homopolymer mixtures (Tuncer, Serkan, Mehmet, & Olgun, 2005). Blend materials from either synthetic or natural polymers alone are not always able to satisfy the complex demands of biomaterials. The success of synthetic polymers as biomaterials may be attributed to their wide range of mechanical properties and the development of transformation processes that allow a variety of different shapes to be easily obtained at a low production cost. Biological polymers present good biocompatibility, but their mechanical properties are often poor. Therefore, biologically important polymeric materials based on blends of synthetic and natural polymers have been studied (Preeti & Jathi, 2010). Alginate (Alg) is a natural biopolymer derived from brown seaweed (Mohan & Nair, 2005). It is hydrophilic, biocompatible, and relatively economical. Alg has been widely used in the medical field for wound dressings, scaffolds for hepatocyte culture, and as a surgical or dental impression material, even if an allergic reaction has occurred on the skin (Ng & Cheng, 2007; Patel, 1993). Carboxymethylcellulose (CMC) is a water-soluble anionic linear polysaccharide and semi-synthetic derivative of cellulose that is produced by the partial substitution of the 2, 3, and 6 hydroxyl groups of cellulose by carboxymethyl groups. CMC polymers are made up of linear β-(1 → 4)-linked glycanes that exhibit polyelectrolyte characteristics due to the presence of weakly acidic groups (Chakraborty, Chakraborty, & Ghosh, 2006; Tong, Xiao, & Lim, 2008). In terms of applications, CMC is an important industrial polymer that has been employed in flocculation, drug reduction, detergents, textiles, paper, foods, and drug formulations (Biswal & Singh, 2004). Researchers have also reported that the addition of CMC produces separate smaller-sized micro fibrils during the growth of Gluconacetobacter. Xylinus (Chen, Chen, Huang, & Lin, 2011; Haigler, Brown, & Benziman, 1980; Hirai, Tsuji, Yamamoto, & Horii, 1998). CMC is primarily used because it has a high viscosity and is both non-toxic and non-allergenic. The numerous hydroxyl and carboxylic groups in CMC enable water binding and moisture sorption properties. Consequently, CMC hydrogels exhibit a high water content and good biodegradability which, when combined with the low cost of the material, has facilitated their use in a wide range of applications (Nie, Liu, Zhan, & Guo, 2004). Generally, the occurrence of specific intermolecular interactions through hydrogen bonding between two or more polymers is responsible for the observed mixing behavior and properties of blends prepared from aqueous solutions (Gaisford, Beezer, Bishop, Walker, & Parsons, 2009). The properties of the resulting blends can be studied so as to expand their range of application in biomedical

* Corresponding author. Tel.: +82 312012565; fax: +82 312026693.
E-mail address: rheeky@khu.ac.kr (K.Y. Rhee).

http://dx.doi.org/10.1016/j.carbpol.2014.03.037
0144-8617/

and pharmaceutical devices. Because both Alg and CMC are water-soluble polymers, they are compatible due to the formation of hydrogen bonds. Numerous reports have been published on the material properties of individual pullulan, alginate, and CMC films (Kawahara et al., 2003; Lee, Chan, Dolzhenko, & Heng, 2006). In addition, blended CMC/Alg films have been investigated as potential composites (Sayeda, Kariman, & Salmawi, 2013). However, no significant improvement was observed in the tensile strength of CMC/Alg films when compared that of the individual component films. Thus, the physical properties of CMC/Alg blend film must be improved to satisfy the demands of specific applications.

The approach of using nano-fillers such as carbon nanotubes, clay, and silica has proven to be effective way to enhance the mechanical, electrical, and thermal properties of polymers (Azeez, Rhee, Park, & Hui, 2013; Azeez, Rhee, Park, Kim, & Jung, 2013; Ha, Rhee, Park, & Lee, 2010; Liu, Phang, Shen, Chow, & Zhang, 2004; Park & Jana, 2003; Park, Kim, Yoo, Rhee, & Lee, 2010; Shaffer & Windle, 1999; Yang et al., 2006). Recently, the application of graphene oxide (GO) as a nano-filler in polymer matrices to prepare polymer nanocomposites has been reported (Yadav, Rhee, Jung, & Park, 2013; Yadav, Jung, et al., 2013; Yadav, Yoo, & Cho, 2013; Yang, Pan, Huang, & Li, 2010; Yu, Ramesh, Itkis, Bekyarova, & Haddon, 2007). Graphene, a single sheet of graphite, has an ideal 2D structure with a monolayer of carbon atoms packed into a honeycomb crystal plane. Using both experimental and theoretical methods, researchers (Geim & Novoselov, 2007; Rao, Sood, Subrahmanyam, & Govindaraj, 2009; Stankovich et al., 2006) have demonstrated the advantages of graphene in the field of materials science. Due to its sp^2 hybrid carbon network and extraordinary mechanical, electronic, and thermal properties, graphene has opened new pathways for the development of a wide range of novel functional materials. Perfect graphene does not exist naturally, but bulk and solution-processable functionalized graphene materials, including GO, can now be prepared (Hao, Qian, Zhang, & Hou, 2008; Li & Kaner, 2008; Park, Jeevananda, Kim, Kim, & Lee, 2008; Park, An, et al., 2008). The large surface area of GO has a number of functional groups (e.g., —OH, —COOH, —O—, and C=O) that make the material hydrophilic and readily dispersible in water as well as some organic solvents (Paredes, Villar-Rodil, Martinez-Alonso, & Tascon, 2008). As a result, graphene-based materials may be easily fabricated by solution casting. Due to its numerous oxygen-containing functional groups and good dispersibility in water, GO is able to interact with the —OH groups of CMC and Alg via hydrogen bonding in an aqueous system. Thus, GO may be viewed as a physical cross-linking agent to obtain interacting polymers, as it can promote miscibility between CMC and Alg molecules, resulting in a compatible blend with enhanced properties. In this work, we report on a simple and environmentally friendly solution mixing-evaporation method for the preparation of blended GO/CMC/Alg composite films. The effects of GO loading on the structure and properties of the blended composites were subsequently investigated.

2. Experimental method

2.1. Materials and methods

Sodium carboxymethyl cellulose (CMC, chemical grade, average molecular weight 250,000 g/mol), sodium alginate (NaAlg, chemical grade, MW 14,000–132,000 g/mol), potassium permanganate (analytical grade), sodium nitrate, and graphite with an average particle size of <20 μm were purchased from Sigma–Aldrich (Korea). Hydrogen peroxide was supplied by the Daejung Chemicals and Metals Company, Ltd. (South Korea), while hydrochloric acid was purchased from Fluka. Sulfuric acid (98%) was purchased from the Junsei Chemical Company (Japan). The water used in this work was distilled and deionized.

2.2. Synthesis of graphene oxide

Graphene oxide (GO) was synthesized from natural graphite flakes (mean particles size of <20 μm) using the Hummers method (Hummers & Offeman, 1958; Ramanathan et al., 2008) with some modification. Briefly, 2 g of graphite and 1 g of $NaNO_3$ were dissolved in 46 mL of concentrated H_2SO_4 in an ice bath. After about 15 min of stirring, 6 g of $KMnO_4$ was gradually added to the suspension under slow stirring in order to hold the reaction temperature below 20 °C. The suspension was stirred for 2 h and then maintained at 35 °C for 30 min. Next, 92 mL of deionized water was slowly poured into the suspension. While the addition of water resulted in a quick increase in temperature, the conditions were controlled such that the temperature remained less than 98 °C. After 15 min, the suspension was further diluted to approximately 280 mL with warm deionized water, after which 20 mL of 30% H_2O_2 was added to remove residual $KMnO_4$ and MnO_2. At this point, the suspension took on a luminous yellow color. The suspension was filtered and washed with a warm 5% HCl aqueous solution and deionized water, respectively, until no sulfates were detected. The pH of the filtrate was subsequently adjusted to 7. The graphene oxide was dried under vacuum at 50 °C to a constant weight and then milled to an ideal particle size. The average size of graphene flakes are 500–5000 nm.

2.3. Preparation of blended GO/CMC/Alg composite films

CMC/Alg composite films containing GO were prepared by a simple solution mixing-evaporation method (Wang, Shen, Zhang, & Tong, 2005). Briefly, 0.01 g of GO was first dissolved in 50 mL of water and sonicated in an ultrasonic bath (Kum Sung Ultrasonic, Korea) for 15 min. Next, a solution containing 0.25 g of CMC, 0.75 g of sodium alginate (Alg), and 49 mL of deionized water was stirred for 5 h using a magnetic stirrer so as to dissolve the CMC and Alg. The GO solution was then added to the CMC/Alg solution, followed by stirring for 5 h. The solution was subsequently degassed for 30 min to remove bubbles, and then poured onto a glass plate at 80 °C under vacuum until dry. Specifics regarding the degassing and curing cycles were determined on the basis of trial and error. Lastly, the dried GO/CMC/Alg composite thin films with an average thickness of 0.04 mm were carefully removed from the glass plate.

The procedure for preparing blended CMC/Alg films was similar to that used for the fabrication of GO/CMC/Alg films, except that no GO was added.

2.4. Characterization

Wide-angle XRD patterns of the composite films were recorded with a Rigaku Rotaflex (RU-200B) X-ray diffractometer using Cu Kα radiation with a Ni filter. The tube current and voltage were 300 mA and 40 kV, respectively, and data from the 2θ angular regions between 5 and 80° were collected. The tensile properties of the composite films were measured at room temperature with a universal test device (Instron 8871), while the surface morphology of the films was analyzed by field emission scanning electron microscopy (FE-SEM, LEO SUPRA 55, Carl Zeiss, Germany). The thermal stability of the films was investigated using a thermogravimetric analysis (TA) instrument (SDT Q600) from 30 °C to 900 °C under a nitrogen atmosphere at a heating rate of 10 °C/min. Dynamic mechanical analysis (DMA) of the nanocomposites was conducted with a dynamic mechanical analyzer (DMA, Q800, TA Company) using tension membrane clamps at a frequency of 1 Hz and a heating rate of 2 °C/min. Raman analysis of the composites

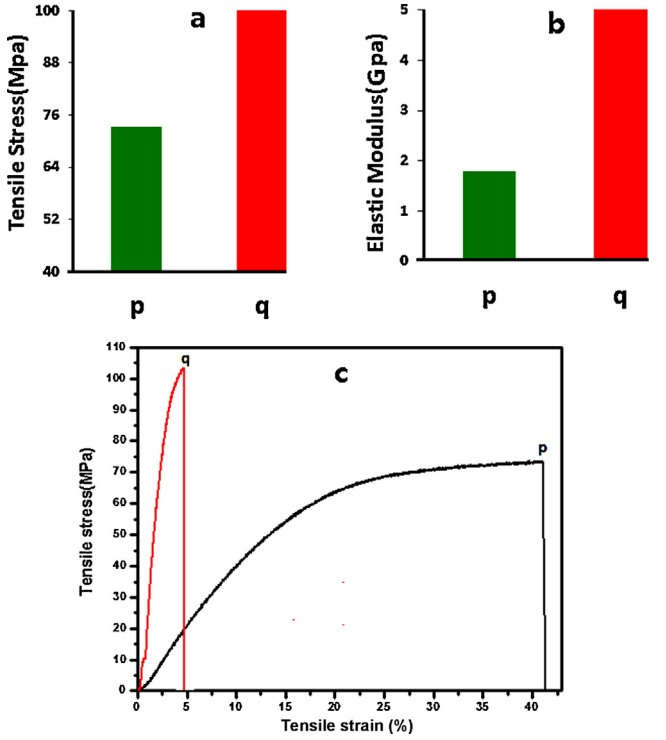

Fig. 1. Tensile strength (a), elastic modulus (b), and stress–strain curves of (*p*) 25%CMC/75%Alg (*q*) 1wt%GO/25%CMC/75%Alg composite blend films.

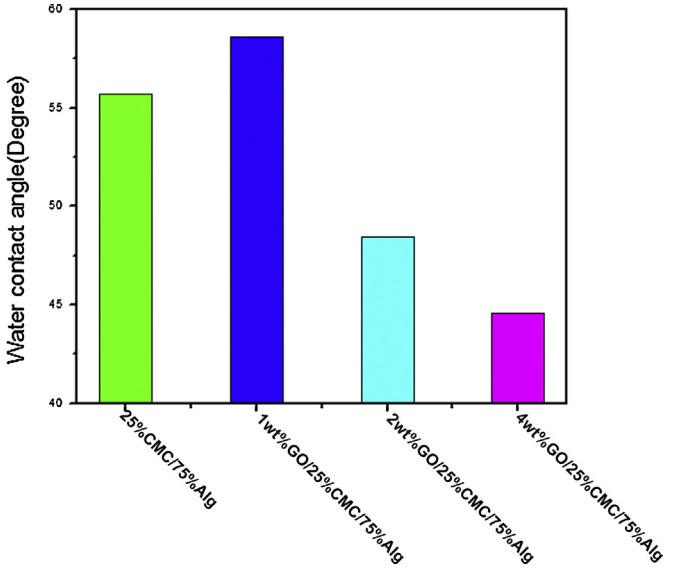

Fig. 2. Water contact angles of 25%CMC/75%Alg, 1wt%GO/25%CMC/75%Alg, 2wt%GO/25%CMC/75%Alg and 4wt%GO/25%CMC/75%Alg composite blend films.

was carried out with a Jasco Raman spectrometer equipped with a CCD detector at a wavelength of 532 nm from 100 to 2000 cm^{-1}; the samples were cut into 5 mm × 10 mm × 0.04 mm strips for the analysis.

3. Results and discussion

3.1. Tensile strength of the composite blend films

A universal test device (Instron 8871) was employed to determine the tensile strength and elastic moduli of the blended composite films at room temperature before and after GO loading. *The length and width of tested blend films were 6 cm and 1 cm, respectively.* Fig. 1 shows typical stress–strain curves of 25%CMC/75%Alg and 1wt%GO/25%CMC/75%Alg composite blend films. The results indicate that loading with a small amount of GO significantly improved the mechanical properties. As evident in Fig. 1c, the stress increased almost linearly with strain in the early stages, and nonlinear behavior was observed for both composites before a maximum stress was reached. The tensile stresses of the 25%CMC/75%Alg and 1wt%GO/25%CMC/75%Alg composite blend films are shown in Fig. 1a. The stress of the GO/25%CMC/75%Alg composite blend film was found to be 40% higher than that of the 25%CMC/75%Alg blend film. The elastic moduli of the samples were determined by measuring the slope in the linear region of the stress–strain curve (Lee, Marroquin, Rhee, Park, & Hui, 2013); the results obtained for the 25%CMC/75%Alg and 1wt%GO/25%CMC/75%Alg composite blend films are shown in Fig. 1b. Similar to the tensile strength results, the elastic modulus also increased with graphene oxide loading. Specifically, the elastic modulus of the 1wt%GO/25%CMC/75%Alg composite blend film was 1128% higher than that of the 25%CMC/75%Alg blend film. These results suggest that GO can improve the strength and stiffness of 25%CMC/75%Alg blend films at the expense of flexibility, as reported in previous studies (Ma, Yu, & Wang, 2008; Yu, Yang, Liu, & Ma, 2009). The improvement in the mechanical properties was due to the good dispersion of GO within the blend film and the ample number of intermolecular hydrogen bond sites formed between the GO and 25%CMC/75%Alg, which resulted in strong interactions among the components. As a result, the miscibility of the components increased and the mechanical properties of the films were greatly improved.

3.2. Hydrophilic behavior of the composite blend films

The hydrophilicity of the composite blend films was analyzed by measuring the water contact angle on the various composites with a FTA-4000 (First Ten Angstroms) contact angle goniometer. Higher hydrophilicity is indicated by a lower water contact angle value (Konyushenko et al., 2006; Park, Jeevananda, et al., 2008; Park, An, et al., 2008). The contact angle of 0wt%GO/25%CMC/75%Alg, 1wt%GO/25%CMC/75%Alg, 2wt%GO/25%CMC/75%Alg, and 4wt%GO/25%CMC/75%Alg composite blend films was 55.69°, 58.63°, 48.46°, and 44.57°, respectively. The 4wt%GO/25%CMC/75%Alg composite film exhibited the highest hydrophilicity among the tested composite blend films (Fig. 2). The increased hydrophilicity of the 4wt%GO/25%CMC/75%Alg composite blend film may be attributed to the presence of a number of hydrophilic functional groups in the graphene oxide. The contact angle of the 1wt%GO/25%CMC/75%Alg composite blend film is lower than that of 0wt%GO/25%CMC/75%Alg composite blend film. The hydrophilicity of the composite blend films can be controlled by adjusting the amount of graphene oxide adsorbed on the 25%CMC/75%Alg surface. The order of water absorbency of the composite blend films may be summarized as follows:

$$4wt\%GO/25\%CMC/75\%Alg > 2wt\%GO/25\%CMC/75\%Alg > 0wt\%GO/25\%CMC/75\%Alg > 1wt\%GO/25\%CMC/75\%Alg$$

3.3. XRD patterns of composite blend films

The XRD patterns of graphite, graphene oxide, and the GO/CMC/Alg composites are presented in Fig. 3. When compared with pristine graphite, the inter-layer spacing of graphene oxide increased from 0.335 to 0.796 nm, indicating a weakening of

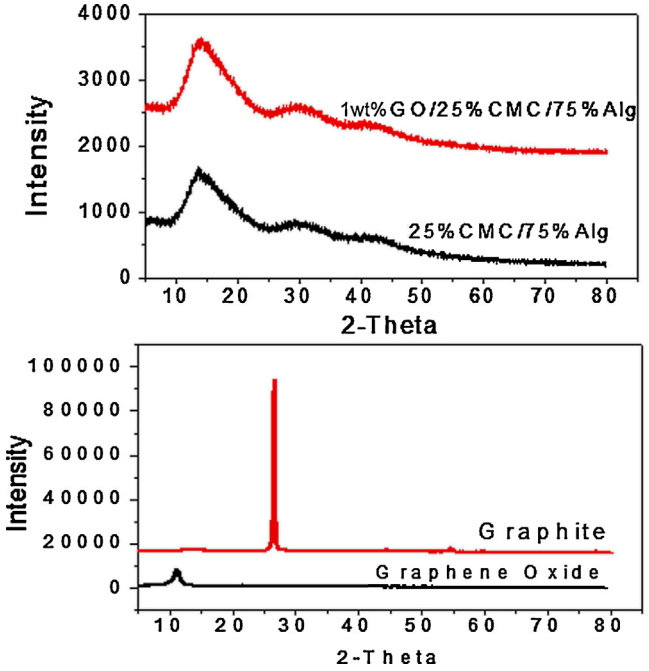

Fig. 3. XRD patterns of GO, graphite, 25%CMC/75%Alg and 1wt%GO/25%CMC/75%Alg composite blend films.

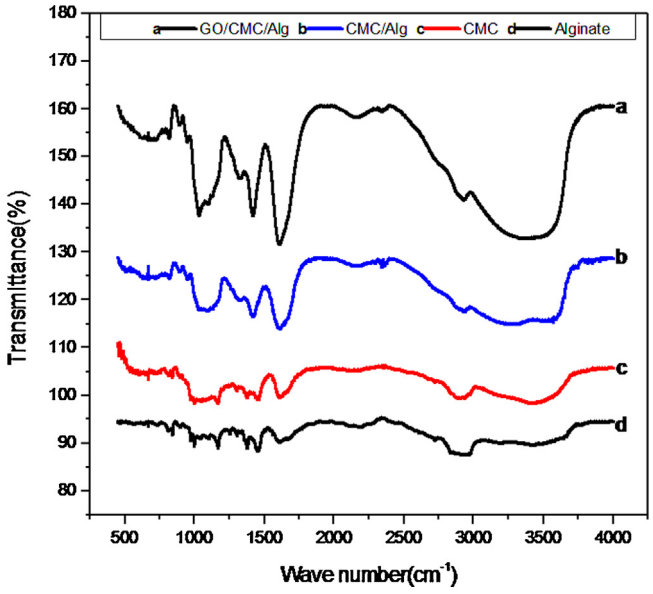

Fig. 4. FT-IR spectra of GO/CMC/Alg, CMC/Alg, and CMC and Alg composite blend films.

inter-layer van der Waals interactions. Therefore, it was relatively easier for graphene oxide to be exfoliated to single or few layer-thick GO by an ultrasonic treatment. The XRD pattern of pure GO showed a strong peak at $2\theta = 11.11$, corresponding to a basal spacing of 7.96 Å. The neat CMC/Alg blend did not show any clear peaks in its XRD pattern due to its amorphous structure. After loading the CMC/Alg matrix with 1 wt% GO, a strong peak from GO at 11.11° (7.96 Å) almost disappeared, while the 2θ values of other diffraction peaks similar to those of pure GO remained unchanged. It can be clearly seen from Fig. 3 that a broadened peak at about 21.67° indicates the existence of an amorphous CMC/Alg structure. The XRD pattern of the 1wt% GO/25%CMC/75%Alg composite blend was nearly the same as that obtained for CMC/Alg, implying that the GO sheets were suitably exfoliated in the CMC/Alg matrix and the amorphous structure of CMC/Alg was not affected by the incorporation of GO. Taken together with the SEM images, it can be inferred that GO was finely dispersed in the polymer matrix.

3.4. FT-IR spectra of the composite blend films

Many previous studies have confirmed that the oxygen atoms in GO exist in —COOH, —C=O, —OH, and —C—O—C groups. The hydrophilic oxygenated functional groups on the surface or at the edge of the GO sheets played a critical role in improving the compatibility between GO and the polymer matrix. The previous research paper (Yadav, Rhee, et al., 2013; Yadav, Jung, et al., 2013; Yadav, Yoo, et al., 2013) shows the FTIR spectra of graphite and graphene oxide; vibrations from graphite are clearly evident. The peaks at 1061.46 cm^{-1}, 1396.46 cm^{-1}, 1729.51 cm^{-1}, and 3396.69 cm^{-1} can be attributed to C—O (ν (epoxy or alkoxy)), O—H (ν (carboxyl)), C=O in carboxylic acid and carbonyl moieties, and O—H (broad coupling ν (hydroxyl)), respectively. The spectrum also showed an absorption peak from the —C=C— group at 1622.67 cm^{-1}, corresponding to the remaining sp^2 characteristics of graphite. From the obtained findings, it can be inferred that graphite was successfully oxidized to form graphene oxide. Furthermore, the abundant oxygen functional groups make the GO sheets strongly hydrophilic, which improves their solubility in water.

From the FTIR spectra of CMC (Fig. 4), a broad absorption band at 3450.61 cm^{-1} is evident due to the stretching frequency of the —OH group. The band at 2928.57 cm^{-1} corresponds to a C—H stretching vibration, while the presence of a strong absorption band at 1597.79 cm^{-1} confirms the presence of COO^- groups. The bands around 1419.07 and 1328.25 cm^{-1} are assigned to —CH_2 scissoring and —OH bending vibrations, respectively, and the band at 1059.95 cm^{-1} is due to >CH—O—CH_2 stretching. The infrared spectrum of alginate showed strong peaks at 3426.19 cm^{-1} due to OH stretching vibrations. For CMC/Alg, the aforementioned peaks at 3450.61 (stretching frequency of the —OH group) and 1597.79 cm^{-1} (COO^- group) in CMC were shifted to 3560.43 and 1615.20 cm^{-1}, respectively. These changes were related to the hydrogen bonding-type interaction in the blends. For the GO/CMC/Alg composite, the peaks at 3560.43 cm^{-1} in CMC/Alg were shifted to 3353.11 cm^{-1}. Such shifting confirms that there is hydrogen bonding-type interactions between the CMC/Alg and GO. Meanwhile, the $^{\delta}$OH bending (1610.78 cm^{-1}) and CH_2 absorption bands (1417.97 cm^{-1}) were shifted to lower wave numbers of 1615.20 and 1419.87 cm^{-1}, respectively, when compared to those of CMC/Alg. The obtained findings indicate that GO acts as a physical cross-linking agent to yield hydrogen bonded interacting polymers, which can in turn promote miscibility between CMC and Alg molecules.

3.5. Morphology analysis

FESEM images of the fracture surfaces of the GO/CMC/Alg composite blends after tensile testing are shown in Fig. 5. The fracture surface images of the GO/CMC/Alg composite blends exhibited maximum sheet stacking due to GO loading. A uniform distribution of GO is observed with the ends of the broken GO exposed on the fracture surface. The observation that most of the GO is broken rather than pulled out from the matrix indicates strong interfacial adhesion between the GO and CMC/Alg matrix. Good dispersion and interfacial stress transfer are important factors for preparing reinforcing composite blends. The TEM of graphene oxide has been reported in the previous paper (Yadav, Rhee, et al., 2013; Yadav, Jung, et al., 2013; Yadav, Yoo, et al., 2013).

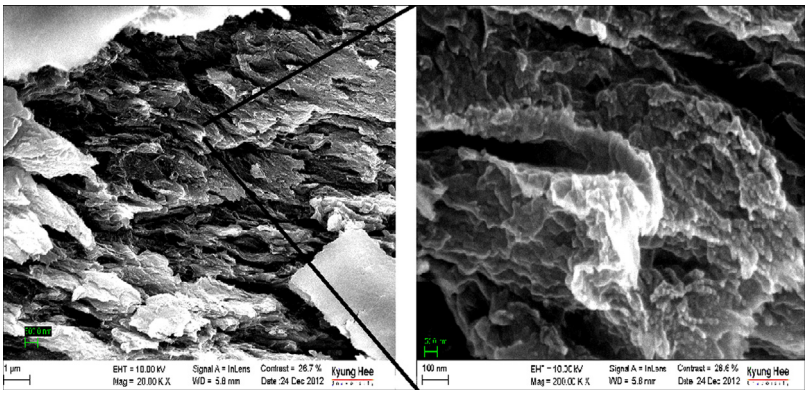

Fig. 5. FESEM images of fracture surfaces of GO/CMC/Alg composite blend films.

3.6. Thermogravimetric analysis

The integral procedural decomposition temperature (IPDT), first proposed by Doyle (1961), accounts for the entire shape of the thermogravimetric analysis (TGA) curve in a single number; it is determined by measuring the area under the TGA curve. The IPDT is correlated with the volatile parts of polymeric materials and thus, it is used to estimate the inherent thermal stability of polymeric materials (Vyazovkin & Sbirrazzuoli, 2006). In the present study, the IPDT was calculated as follows:

$$\text{IPDT}(^\circ\text{C}) = A^*K^*(T_f - T_i) + T_i \quad (1)$$

$$A^* = \frac{S_1 + S_2}{S_1 + S_2 + S_3} \quad (2)$$

$$K^* = \frac{S_1 + S_2}{S_1} \quad (3)$$

where A^* is the area ratio of the total experimental curve defined by the entire TGA thermogram, T_i is the initial experimental temperature, and T_f is the final experimental temperature. Representations of S_1, S_2, and S_3 for calculating A^* and K^* are given in previous works (Yadav & Rhee, 2012). The TGA and DSC curve of graphite and graphene oxide has been reported in the previous published paper (Yadav, Rhee, et al., 2013; Yadav, Jung, et al., 2013; Yadav, Yoo, et al., 2013).The TGA results confirmed that pristine graphite was very stable, as no observable weight loss was detected upon heating to 900 °C. However, GO was more thermally unstable than graphite, undergoing a three-step degradation process. Graphene oxide lost 15% of its weight up to 176 °C, possibly due to the evaporation of adsorbed water and the thermal decomposition of oxygen-containing functional groups such as carboxyls, hydroxyls, epoxies, nitrogen dioxide, and ketones. The weight loss rate of GO increased as the temperature was increased from 176 °C to 250 °C, and then decreased thereafter. A maximum weight loss of about 57.5 wt% was observed at approximately 587 °C, suggesting the presence of structural defects in the GO due to strong acid oxidation. Upon comparing the thermograms of graphite and graphene oxide, the IPDTs of graphite and graphene oxide were calculated as 91,826 and 812, respectively, indicating that graphite is more thermally stable than graphene oxide. The TGA curves of CMC/Alg and GO/CMC/Alg are shown in Fig. 6; multi-step degradation was observed for both specimens. The weight loss of 7.92 wt% at approximately 100 °C may have been due to a loss of absorbed water, which began at approximately 50 °C. The polymer decomposition temperature (PDT) was found to be approximately 150 °C. The weight loss rate increased with increasing temperature from 218 °C to 281 °C, and then decreased thereafter. A maximum weight loss of approximately 76 wt% was observed at about 800 °C. The degradation of CMC/Alg occurred in four steps rather than one. Specifically, CMC/Alg degraded differently in the temperature ranges of 32–100, 200–306, 306–516, and 760–838 °C, with T_{max} values of 57, 241, 386, and 810 °C in the four-step degradation, respectively (DTG data in Fig. 6). The thermal stability values of the CMC/Alg and GO/CMC/Alg composites were determined by calculating the IPDT values. The IPDT and final decomposition temperature (FDT) of the CMC/Alg films were 631 °C and 850 °C, respectively. In the case of GO/CMC/Alg, a weight loss of 11% at approximately 100 °C may have been due to a loss of absorbed water. While the polymer decomposition temperature (PDT) was identified as 219 °C, degradation of the GO/CMC/Alg (0.5 wt%) began at approximately 200 °C (Fig. 6). The rate of weight loss increased with increasing temperature from 219 °C to 279 °C and, then decreased thereafter. A maximum weight loss of 77.31 wt% was observed at approximately 806 °C. Degradation of the GO/CMC/Alg occurred in four steps at 28–110, 201–308, 315–548 and 753–888 °C, with T_{max} values of 57, 240, 386, and 810 °C, respectively (DTG data, Fig. 6). The differential scanning calorimetry (DSC) curves of the CMC/Alg and GO/CMC/Alg composite films are also shown in Fig. 6. The IPDT and FDT of GO/CMC/Alg (0.5 wt%) were 622 °C and 800 °C, respectively. A comparison of the thermograms of CMC/Alg and GO/CMC/Alg showed that the FDT and IPDT values were higher for GO/CMC/Alg, indicating that GO/CMC/Alg is less thermally stable than CMC/Alg.

3.7. Viscoelastic properties

The variation in dynamical mechanical thermal properties of the composite blend (1wt%GO/25%CMC/75%Alg) has been studied to determine the change in glass transition temperature and the viscoelastic stability of the polymer on incorporation of the graphene oxide enhancement. The storage modulus (E') of the pure blend polymer increases with the increase in graphene oxide content, and its temperature variation is depicted in Fig. 7. The storage modulus at 50 °C is 3.08 GPa for the pure blend polymer and increases to 3.85 GPa for the 1wt%GO/25%CMC/75%Alg composite blend film. Initially with the increase in temperature, the storage modulus drops linearly in the rubbery region from 110 °C till 160 °C for the pure blend polymer. The rate of decrease is considerably lower for composite blend with graphene oxide in this region. Increasing the temperature increases the segmental motion of the pure blend polymer and there is a sharp increase in $\tan\delta$ which corresponds to the α relaxation temperature associated with the glass transition temperature T_g (Fig. 7). In the pure blend polymer this is seen at 155 °C, and enhanced pure blend polymer graphene interaction causes it to reach 166 °C for the 1wt%GO/25%CMC/75%Alg composite blend film. The addition of graphene oxide restricts the mobility of the chains, and thus the glass transition temperature increases. But effectively the loss factor ($\tan\delta$) reduces, which is the ratio of the loss modulus to the storage modulus, showing enhanced

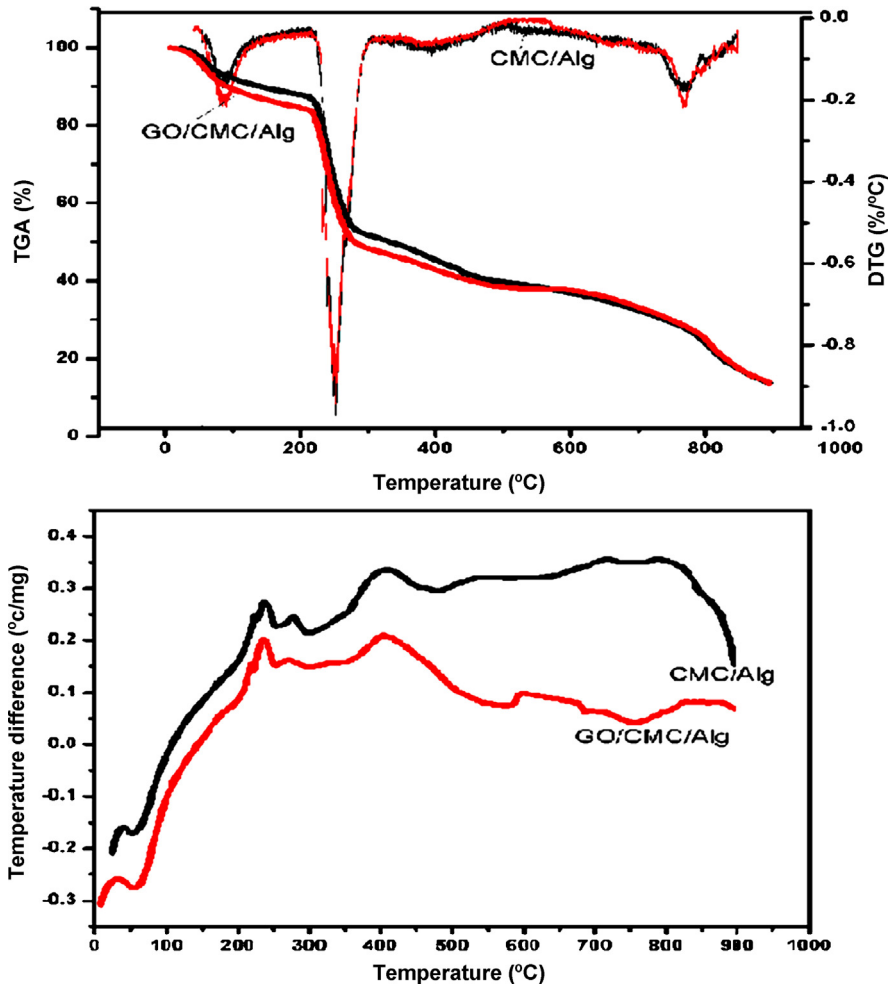

Fig. 6. TGA, DTG, and DSC of CMC/Alg and GO/CMC/Alg composite blend films.

ceramic nature of the blend polymer hybrids (Fig. 7). The value of tan δ progressively decreases from 0.18 for the pure polymer to 0.11 for the 1wt%GO/25%CMC/75%Alg composite blend film. The viscoelastic data is presented in Table 1.

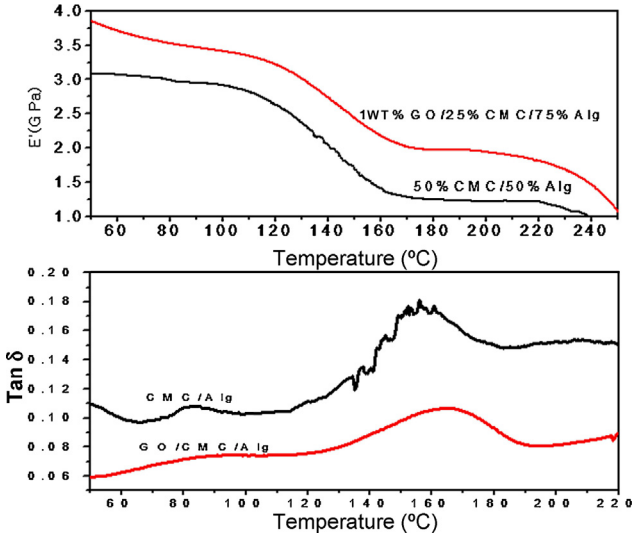

Fig. 7. Storage modulus (E') and glass transition temperature (T_g) of CMC/Alg and GO/CMC/Alg composite blend films.

3.8. Raman spectroscopy

Raman spectroscopy can provide valuable information regarding the graphitic structure, specifically, whether the carbon-based nanoparticles are composed of amorphous or disordered carbon. Moreover, Raman spectroscopy can confirm structural changes of the graphite before and after oxidation. In this study, pristine graphite showed three characteristic peaks at 1363.52 (D-band, C—C), 1583.25 (G-band, C=C), and 2732.47 cm^{-1} (2D-band). The Raman spectrum of GO (Fig. 8) exhibited two prominent peaks at 1618.88 cm^{-1} and 1371.93 cm^{-1}, which correspond to the well-documented G and D bands, respectively. The D band arises due to defects in the graphene oxide and staging disorder, while the G band is related to the graphitic hexagon-pinch mode (Mao et al., 2012). The intensities of the D and G bands can be used to determine the degree of defects, which is estimated as the I_D/I_G ratio. In the present study, the I_D/I_G ratio was 0.15, indicating that the graphite had a nearly defect-free structure. When we

Table 1
Viscoelastic properties of composite blend (GO/CMC/Alg).

Graphene oxide (wt%)	1wts%GO/25%CMC/75%ALG		
	Storage modulus (GPa) at 50 °C	T_g (°C)	tan delta (δ)
0	3.08	155	0.18
1	3.8	166	0.11

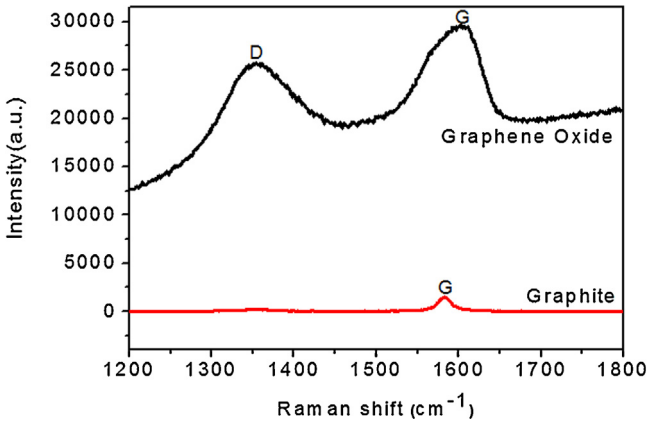

Fig. 8. Raman spectrum of graphite and graphene oxide.

compared the I_D/I_G ratios of pristine graphite and graphene oxide, it was found that the graphene oxide had a much higher I_D/I_G ratio of 0.89, indicating the presence of defects.

4. Conclusion

A series of composite blend films that consisted of CMC, Alg and GO were prepared by a simple solution mixing-evaporation method. The results from FTIR indicated that the GO improved miscibility between CMC and Alg, which results from hydrogen bonding interaction between GO and CMC/Alg matrix, and the GO does play the role of physical cross-linking points. In addition, XRD analysis of GO/CMC/Alg composite blend film showed that the GO sheets were well exfoliated in the CMC/Alg matrix. Compared to the tensile strength of the CMC/Alg matrix, it can be seen that the tensile strength and young's modulus of the composite films increased by 40% and 1128% with 1 wt% GO loading levels, respectively. TGA results suggested that GO/CMC/Alg is less thermally stable than CMC/Alg alone. Furthermore, the GO/CMC/Alg composite blend film showed a higher storage modulus (E') than the CMC/Alg blend film.

Acknowledgements

This work was supported by the Basic Science Research Program through the National Research Foundation of Korea (NRF) funded by the Ministry of Education, Science and Technology (project number:2013R1A1A2A10063466).

References

Azeez, A. A., Rhee, K. Y., Park, S. J., & Hui, D. (2013). Epoxy clay nanocomposites processing, properties and applications: A review. *Composites Part B: Engineering*, *45*, 308–320.

Azeez, A. A., Rhee, K. Y., Park, S. J., Kim, H. J., & Jung, D. H. (2013). Application of cryomilling to enhance material properties of carbon nanotube reinforced chitosan nanocomposites. *Composites Part B: Engineering*, *50*, 127–134.

Biswal, D. R., & Singh, R. P. (2004). Characterisation of carboxymethyl cellulose and polyacrylamide graftcopolymer. *Carbohydrate Polymer*, *57*, 379–387.

Chakraborty, T., Chakraborty, I., & Ghosh, S. (2006). Sodium carboxymethylcellulose–CTAB interaction: A detailed thermodynamic study of polymer–surfactant interaction with opposite charges. *Langmuir*, *22*, 9905–9913.

Chen, H. H., Chen, L. C., Huang, H. C., & Lin, S. B. (2011). In situ modification of bacterial cellulose nanostructure by adding CMC during the growth of *Gluconacetobacter xylinus*. *Cellulose*, *18*, 1573–1583.

Doyle, C. D. (1961). Estimating thermal stability of experimental polymers by empirical thermogravimetric analysis. *Analytical Chemistry*, *33*, 77.

Gaisford, S., Beezer, A. E., Bishop, A. H., Walker, M., & Parsons, D. (2009). An in vitro method for the quantitative determination of the antimicrobial efficacy of silver-containing wound dressings. *International Journal of Pharmaceutics*, *366*, 111.

Geim, A. K., & Novoselov, K. S. (2007). The rise of graphene. *Nature Materials*, *6*, 183–191.

Ha, S. R., Rhee, K. Y., Park, S. J., & Lee, J. H. (2010). Temperature effects on the fracture behavior and tensile properties of silane-treated clay/epoxy nanocomposites. *Composites Part B: Engineering*, *41*, 602–607.

Haigler, C. H., Brown, R. M., Jr., & Benziman, M. (1980). Calcofluor white ST alters the in vivo assembly of cellulose microfibrils. *Science*, *210*, 903–906.

Hao, R., Qian, W., Zhang, L. H., & Hou, Y. L. (2008). Aqueous dispersions of TCNQ anion-stabilized graphene sheets. *Chemical Communications*, *48*, 6576–6578.

Hirai, A., Tsuji, M., Yamamoto, H., & Horii, F. (1998). In situ crystallization of bacterial cellulose III. Influences of different polymeric additives on the formation of micro fibrils as revealed by transmission electron microscopy. *Cellulose*, *5*, 201–213.

Hummers, W. S., Jr., & Offeman, R. E. (1958). Preparation of graphite oxide. *Journal of the American Chemical Society*, *80*, 1339.

Kawahara, M., Mizutani, K., Suzuki, S., Kitamura, S., Fukada, H., & Yui, T. (2003). Dependence of the mechanical properties of a pollulan film on the preparation temperature. *Bioscience, Biotechnology, and Biochemistry*, *67*, 893.

Konyushenko, E. N., Stejskal, J., Trchova, M., Hradil, J., Kovařova, J., Prokeš, J., et al. (2006). Multi-wall carbon nanotubes coated with polyaniline. *Polymer*, *47*, 5715–5723.

Lee, H. Y., Chan, I. W., Dolzhenko, A., & Heng, P. W. S. (2006). Influence of viscosity and uronic acid composition of alginates on the properties of alginates films and microspheres produced by emulsification. *Journal of Microencapsulation*, *23*, 912.

Lee, J. H., Marroquin, J., Rhee, K. Y., Park, S. J., & Hui, D. (2013). Cryomilling application of graphene to improve material properties of graphene/chitosan nanocomposites. *Composites: Part B. Engineering*, *45*, 682–687.

Li, D., & Kaner, R. B. (2008). Graphene-based materials. *Science*, *320*, 1170–1171.

Liu, T., Phang, I. Y., Shen, L., Chow, S. Y., & Zhang, W. D. (2004). Morphology and mechanical properties of multiwalled carbon nanotubes reinforced nylon-6. *Macromolecules*, *37*, 7214.

Ma, X. F., Yu, J. G., & Wang, N. (2008). Glycerol plasticized-starch/multiwall carbon nanotube composites for electroactive polymers. *Composites Science and Technology*, *68*, 268–273.

Mao, A., Zhang, D., Jin, X., Gu, X., Wei, X., Yang, G., et al. (2012). Synthesis of graphene oxide sheets decorated by silver nanoparticles in organic phase and their catalytic activity. *Journal of Physics and Chemistry of Solids*, *73*, 982–986.

Mohan, N., & Nair, P. D. (2005). Novel porous, polysaccharide scaffolds for tissue engineering applications. *Trends in Biomaterials & Artificial Organs*, *18*, 219.

Ng, R. W., & Cheng, Y. L. (2007). Calcium alginate dressing related hyperclacaemia. *Journal of Burn Care & Research*, *28*, 203.

Nie, H., Liu, M., Zhan, F., & Guo, M. (2004). Factors on the preparation of carboxymethycellulose hydrogel and its degradation behavior in soil. *Carbohydrate Polymer*, *58*, 185–189.

Paredes, J. I., Villar-Rodil, S., Martinez-Alonso, A., & Tascon, J. M. D. (2008). Graphene oxide dispersions in organic solvents. *Langmuir*, *24*, 10560–10564.

Park, J. H., & Jana, S. C. (2003). The relationship between nano- and micro-structures and mechanical properties in PMMA–epoxy–nanoclay composites. *Polymer*, *44*, 2091.

Park, O.-K., Jeevananda, T., Kim, N. H., Kim, S. I., & Lee, J. H. (2008). Effects of surface modification on the dispersion and electrical conductivity of carbon nanotube/polyaniline composites. *Scripta Mater*, *60*, 551–554.

Park, O. K., Kim, N. H., Yoo, G. H., Rhee, K. Y., & Lee, J. H. (2010). Effects of the surface treatment on the properties of polyaniline coated carbon nanotubes/epoxy composites. *Composites: Part B. Engineering*, *41*, 2–7.

Park, S., An, J. H., Piner, R. D., Jung, I., Yang, D. X., Velamakanni, A., et al. (2008). Aqueous suspension and characterization of chemically modified graphene sheets. *Chemistry of Materials*, *20*, 6592–6594.

Patel, H. A. (1993). Preparing an alginate containing wound dressing. US Pat 5:470.

Preeti, K., & Jathi, K. (2010). Preparation and evaluation of polyvinyl alcohol transdermal membranes of salbutamol sulphate. *International Journal of Current Pharmaceutical Research*, *2*, 13–16.

Ramanathan, T., Abdala, A., Stankovich, A., Dikin, S., Herrera, D. A., Alonso, M., et al. (2008). Functionalized graphene sheets for polymer nanocomposites. *Nature Nanotechnology*, *3*, 327–331.

Rao, C. N. R., Sood, A. K., Subrahmanyam, K. S., & Govindaraj, A. (2009). Graphene: The new two-dimensional nanomaterial. *Angewandte Chemie International Edition*, *48*, 7752–7777.

Sayeda, M. I., Kariman, M., & Salmawi, El. (2013). Preparation and properties of carboxymethyl cellulose (CMC)/sodium alginate (SA) blends induced by gamma irradiation. *Journal of Polymers and the Environment*, *21*(2), 520–527.

Shaffer, M. S. P., & Windle, A. H. (1999). Fabrication and characterization of carbon nanotube/poly(vinyl alcohol) composites. *Advanced Materials*, *11*, 937.

Stankovich, S., Dikin, D. A., Dommett, G. H. B., Kohlhaas, K. M., Zimney, E. J., Stach, E. A., et al. (2006). Graphene-based composite materials. *Nature*, *442*, 282–286.

Tong, Q., Xiao, Q., & Lim, L. T. (2008). Preparation and properties of pullulan–alginate–carboxymethylcellulose blend films. *Food Research International*, *41*, 1007–1014.

Tuncer, C., Serkan, D., Mehmet, S. E., & Olgun, G. (2005). Poly(ethylene oxide) and its blend with sodium alginate. *Polymer*, *46*, 10750.

Vyazovkin, S., & Sbirrazzuoli, N. (2006). Isoconversional kinetic analysis of thermally stimulated processes in polymers. *Macromolecular Rapid Communications*, *27*, 1515–1532.

Wang, S., Shen, L., Zhang, W., & Tong, Y. (2005). Preparation and mechanical properties of chitosan/carbon nanotubes composites. *Biomacromolecules*, *6*, 3067–3072.

Yadav, M., & Rhee, K. Y. (2012). Superabsorbent nanocomposite (alginate-g-PAMPS/MMT): Synthesis, characterization and swelling behavior. *Carbohydrate Polymers*, *90*, 165–173.

Yadav, M., Rhee, K. Y., Jung, I. H., & Park, S. J. (2013). Eco-friendly synthesis, characterization and properties of a sodium carboxymethyl cellulose/graphene oxide nanocomposite film. *Cellulose*, *20*, 687–698.

Yadav, S. K., Jung, Y. C., Kim, J. H., Ko, Y. I., Ryu, H. J., Yadav, M., et al. (2013). Mechanically robust, electrically conductive biocomposite films using antimicrobial chitosan-functionalized graphenes. *Particle & Particle Systems Characterization*, *30*, 721–727.

Yadav, S. K., Yoo, H. J., & Cho, J. W. (2013). Click coupled graphene for fabrication of high-performance polymer nanocomposites. *Journal of Polymer Science Part B: Polymer Physics*, *51*, 39–47.

Yang, H., Zhang, Q., Guo, M., Wang, C., Du, R., & Fu, Q. (2006). Study on the phase structures and toughnening mechanism in PP/EPDM/SiO_2 ternary composites. *Polymer*, *47*, 2106.

Yang, Q., Pan, X., Huang, F., & Li, K. (2010). Fabrication of high-concentration and stable aqueous suspensions of graphene nanosheets by non covalent functionalization with lignin and cellulose derivatives. *Journal of Physical Chemistry C*, *114*, 3811–3816.

Yu, A. P., Ramesh, P., Itkis, M. E., Bekyarova, E., & Haddon, R. C. (2007). Graphite nanoplatelet-epoxy composite thermal interface materials. *Journal of Physical Chemistry C*, *111*, 7565–7569.

Yu, J., Yang, J., Liu, B., & Ma, X. (2009). Preparation and characterization of glycerol plasticized-pea starch/ZnO–carboxymethylcellulose sodium nanocomposites. *Bioresource Technology*, *100*, 2832–2841.